Published online 9 July 2019

Nucleic Acids Research, 2019, Vol. 47, No. 14 ***7199–7212***
doi: 10.1093/nar/gkz565

Single-molecule analysis of i-motif within self-assembled DNA duplexes and nanocircles

Anoja Megalathan[1], Bobby D. Cox[2], Peter D. Wilkerson[2], Anisa Kaur[1], Kumar Sapkota[1], Joseph E. Reiner[2] and Soma Dhakal[1,*]

[1]Department of Chemistry, Virginia Commonwealth University, 1001 West Main Street, Richmond, VA 23284, USA and [2]Department of Physics, Virginia Commonwealth University, 701 West Grace Street, Richmond, VA 23284, USA

Received November 13, 2018; Revised June 13, 2019; Editorial Decision June 16, 2019; Accepted July 04, 2019

ABSTRACT

The cytosine (C)-rich sequences that can fold into tetraplex structures known as i-motif are prevalent in genomic DNA. Recent studies of i-motif–forming sequences have shown increasing evidence of their roles in gene regulation. However, most of these studies have been performed in short single-stranded oligonucleotides, far from the intracellular environment. In cells, i-motif–forming sequences are flanked by DNA duplexes and packed in the genome. Therefore, exploring the conformational dynamics and kinetics of i-motif under such topologically constrained environments is highly relevant in predicting their biological roles. Using single-molecule fluorescence analysis of self-assembled DNA duplexes and nanocircles, we show that the topological environments play a key role on i-motif stability and dynamics. While the human telomere sequence $(C_3TAA)_3C_3$ assumes i-motif structure at pH 5.5 regardless of topological constraint, it undergoes conformational dynamics among unfolded, partially folded and fully folded states at pH 6.5. The lifetimes of i-motif and the partially folded state at pH 6.5 were determined to be 6 ± 2 and 31 ± 11 s, respectively. Consistent with the partially folded state observed in fluorescence analysis, interrogation of current versus time traces obtained from nanopore analysis at pH 6.5 shows long-lived shallow blockades with a mean lifetime of 25 ± 6 s. Such lifetimes are sufficient for the i-motif and partially folded states to interact with proteins to modulate cellular processes.

INTRODUCTION

Cytosine-rich (C-rich) sequences that can fold into tetraplex helical structures known as i-motif (1,2) are prevalent in genomic DNA (3,4), and there exists experimental evidence for the role of i-motif in various biological processes such as regulation of gene expression (5–9) and replication (10–12). More importantly, recent biochemical studies have shown experimental evidence for the existence of i-motif at physiological pH (3,4) and in human nuclei (11,13). While there are very few studies on the i-motif under biological context such as molecular crowding (14–16) and negative superhelicity (17–19), *in vitro* biophysical and spectroscopic studies, such as NMR (2,20,21), UV/Vis, circular dichroism (CD) (8,22,23), nanopore (24), Förster resonance energy transfer (FRET) (25) and optical tweezers (5,26) have contributed significantly in understanding how their intrinsic properties relate to these biological functions (23,25,27–30). However, *in vitro* studies so far have been mainly carried out using short oligonucleotides as models under isolation far from biologically relevant environments and have been explored for various applications such as pH sensors (31,32), nanomechanical machines (33–38), and other analytical and biomedical applications (39–41). Much different from isolated oligonucleotide, i-motif sequences in cells are flanked by long stretches of duplex DNA, which could change the topology as well as the thermodynamic and kinetic properties of i-motif (17,42).

While G-quadruplexes (tetraplex structures that are formed in G-rich sequences) have been explored extensively under various mechanically and electrophoretically constrained environments using single-molecule experiments such as optical tweezers and nanopores (17,19,43,44), fewer studies have been done on i-motif (12). Previous studies on i-motif demonstrated a slow folding/unfolding kinetics of the structure and showed that the dynamics heavily rely on the sequences (20), solution pH (45,46) and whether or not the complementary G-rich strand is present (46). For example, the association equilibrium constant of i-motif is decreased by over 20-fold in the presence of complementary G-rich strand. Using a 1:1 mixture of G-rich and C-rich sequences Phan and Mergny showed that the sequences predominantly fold into G-quadruplex and i-motif structures

*To whom correspondence should be addressed. Tel: +1 804 828 8422; Fax: +1 804 828 8599; Email: sndhakal@vcu.edu

at acidic pH (21). However, they showed that at pH 7.0 and 100 mM NaCl, DNA duplex was the predominant species. More interestingly, recent studies have shown that the other intracellular factors such as crowding (15,16) and negative superhelicity (17) destabilize the DNA duplexes and hence favor the formation of i-motif in the C-rich strand and G-quadruplex in the complementary G-rich strand even at near neutral pH. Therefore, determining thermodynamic and kinetic properties of i-motif under naturally occurring environments where i-motif forming sequences have fewer degrees of freedom and experience topological constraints (18,26,47,48) would provide unprecedented insights toward exploiting these structures for biological as well as material applications (17,49,50). Further, with the recent finding that i-motif can form inside cells (11,13), it is critically important to characterize the i-motif under such molecularly constrained and strained conditions (49).

In this study, we demonstrate self-assembled DNA nanostructures (Figure 1A) as molecular tools to study i-motif dynamics under restricted and topologically strained environments. Using fluorescently labeled DNA nanoassemblies, we systematically compared the folding and conformational dynamics of a 21-mer (5′-$(CCCTAA)_3CCC$) human telomere (hTel) sequence present in either the terminal position of a DNA duplex, within DNA duplexes or embedded within DNA nanocircles (Figure 1 and see Supplementary Table S1 for sequences). The size of the nanocircles used in this study closely resembles the DNA topology inside cells where the dsDNA wraps around the histone in a helical fashion using ∼146 bp for 1.65 turns (∼89 bp for one full turn) (51). Further, our choice of hTel i-motif as a model sequence is motivated by its known structure and implications in cancer diseases and aging (27). First, using smFRET, we show that the hTel sequence assumes a fully folded i-motif structure at pH 5.5 and remains unstructured at pH 9.0. However, at slightly acidic pH (pH 6.5) the sequence undergoes equilibrium dynamics between i-motif, partially folded and fully unfolded conformations. The kinetics of switching between these species is different in different nanoassemblies, revealing the effect of topological strain on the conformational dynamics. Second, using α-hemolysin (α-HL)-based nanopore analysis of the core 21-mer hTel sequence without overhangs shows pH-dependent conformational transitions that are consistent with smFRET results. Interrogation of current versus time (*i–t*) traces at pH 5.5 show characteristic current blockades consistent with formation of the fully folded state. Similar analysis at pH 6.5 shows long-lived shallow blockades that are consistent with the partially folded state observed in smFRET and CD. While previous studies on telomeric i-motif using α-HL nanopore (24) and smFRET (45) have provided some insights into the switching kinetics between fully folded and unfolded states, our study has provided more detailed insights into the folding and dynamics of various species including the partially folded state with and without topological constraint. The lifetimes of i-motif and partially folded species of an hTel C-rich sequence observed here are sufficiently long to affect enzymes operating on DNA (12,52–55).

MATERIALS AND METHODS

Chemicals

Tris(hydroxymethyl)-aminomethane (tris), boric acid, acetic acid, KCl, EDTA, acrylamide/bisacrylamide (19:1), ammonium persulfate (prepared as a 10% solution in sterile water and stored at 4°C) and tetramethylethylenediamine (TEMED) were purchased from Fisher Scientific. Magnesium chloride hexahydrate, 6-hydroxy-2,5,7,8-tetramethylchroman-2-carboxylic acid (trolox) and 30% ammonia water were purchased from Arcos Organics. Sodium chloride, ethidium bromide, streptavidin, protocatechuic acid (PCA), MES monohydrate, sodium hydroxide and hydrogen peroxide were purchased from VWR. Bovine serum albumin (BSA) was purchased from New England Biolabs (NEB). Protocatechuate 3,4-dioxygenase (PCD) was purchased from MP Biomedicals, and suspended in a pH 8.0 PCD buffer (100 mM Tris-HCl, 50 mM KCl, 1 mM EDTA, 50% glycerol) at 0.2 μM, sterile filtered and stored at −20°C. Biotin-modified BSA was purchased from Peirce, dissolved in sterile H_2O at 1 mg/ml, sterile filtered and stored at −20°C. Catalase from bovine liver and glucose oxidase from *Asperigillus niger* were purchased from Sigma Aldrich. For nanopore experiments, hexadecane, pentane, potassium chloride and Tris were purchased from Sigma-Aldrich. 1,2 diphytanoyl-sn-glycero-3-phosphocholine (DPhyPC) lipid was purchased from Avanti polar lipids. Alpha toxin from *Staphylococcus Aureus* was purchased from List Biological.

DNA nanoassemblies

All of the DNA oligos (modified and unmodified) were purchased from Integrated DNA Technologies (IDT) and stored at −20°C until needed. The biotin, Cy3 and Cy5 modified oligos were purchased HPLC purified. We designed our nanocircles according to the methods described in previous publications (38,50). The DNA assemblies were prepared by thermal annealing of the constituent ssDNA oligos (Supplementary Table S1) at 1 μM concentrations in 1 × TAE-Mg buffer, pH 7.4 (40 mM Tris, 20 mM acetic acid, 1 mM EDTA, 10 mM Mg^{2+}). The thermal annealing was carried out by ramping the temperature of the solution from 95 to 4°C in a thermal cycler (Supplementary Table S2) and checked with gel mobility shift assay as described below.

Electrophoretic mobility shift assay (EMSA)

The formation of nanoassemblies was analyzed by native polyacrylamide gel electrophoresis (PAGE). A 6% native polyacrylamide gel was cast in 1× TBE (89 mM Tris, 89 mM boric acid, 2 mM EDTA) and immersed in a buffer system consisting of 1 TBE at pH 7.4. The 100 base-pair ladder was used as a molecular weight (MW) marker. The gel apparatus was run at 50 V for 1 h 40 min before being stained with ethidium bromide (EtBr) and imaged using a UV transilluminator (254 nm).

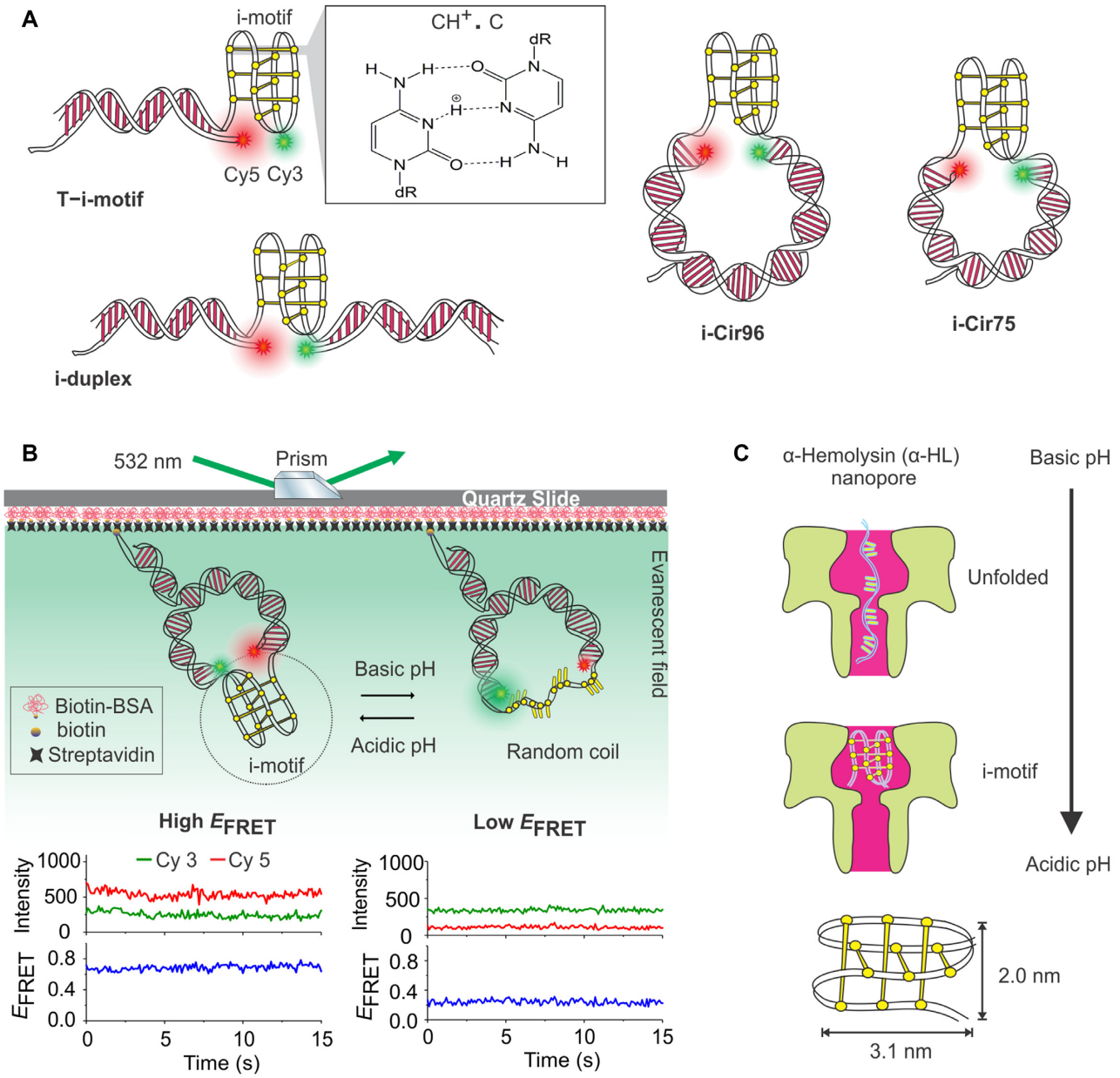

Figure 1. Schematic representation of DNA nanoassemblies and experimental setup for smFRET and α-hemolysin nanopore. E_{FRET} represents the FRET efficiency. (**A**) DNA constructs with the hTel i-motif either at the terminal position of a dsDNA (*T-i-motif*) or embedded within a DNA duplex (*i-duplex*), 96 bp circle (*i-Cir96*) and 75 bp circle (*i-Cir75*). The i-motif line drawing is based on PDB 1ELN. Note that the PDB structure was obtained without 5′-end thymine overhang. The hemiprotonation of cytosine$^+$-cytosine (CH^+•C) is shown in T-i-motif. Cy3 and Cy5 fluorophores are shown in green and red, respectively. (**B**) Experimental setup for the smFRET analysis of hTel i-motif. The biotin-labeled DNA nanoassemblies were surface-immobilized on a quartz slide through biotin/streptavidin interaction. It is expected that the hTel sequence folds into an i-motif structure (high E_{FRET}) at acidic pH and unfolds to random coil (low E_{FRET}) at basic pH. The typical intensity–time (*i*–*t*) traces and the corresponding smFRET traces are shown for the fully folded (high E_{FRET}, left panel) and fully unfolded states (low E_{FRET}, right panel). (**C**) Nanopore analysis of hTel sequence at various pH using α-hemolysin. The i-motif strand translocates through the pore when fully unfolded but stays in the nanopore when fully folded into i-motif structure.

Circular dichroism (CD)

DNA oligonucleotides prepared in a concentration of ∼10 μM in 1× TAE (pH 6.0, 6.5, 7.0, 7.4 and 9.0) and MES buffer (pH 5.5) were heated at 95°C for 5 min and transferred to an ice bath. The CD spectra were collected (after ∼1 h of incubation at room temperature) at a scan rate of 100 nm/min in a 1 mm quartz cuvette at room temperature with a Jasco-1500 spectrometer. The reported mean spectra are the average of three scans, blank corrected and smoothed using a Savitzky–Golay function.

Single-molecule florescence microscopy

Preparation and functionalization of flow cell. The flow cell was prepared using standard microscope quartz slides and

cover slips as described in the Supplementary Data. Thus, prepared flow cells were functionalized by sequential incubation with 1 mg/ml biotinylated BSA (bBSA) for ∼5 min and 0.2 mg/ml streptavidin for ∼2 min. Then, the flow cells were flushed with ∼300 μl of 1 × TAE-Mg buffer.

Single-molecule imaging of i-motif nanoassemblies. The bBSA/streptavidin modified flow cell was incubated with 20–30 pM solution of i-motif nanoassemblies dispersed in a given buffer for ∼1 min before being flushed with the same buffer to remove the unbound nanoassemblies. A 300 μl solution of imaging buffer (1× MES-10 mM Mg for pH 5.5; 1× TAE-10 mM Mg buffer for pH 6.5, 7.4 and 9.0) containing 2× oxygen scavenger system (OSS) was injected and incubated for ∼5 min before recording the movies. Of note, since the same OSS system did not work for the entire pH range, OSS solution consisting of 5 mM PCA, 50 nM PCD and 2 mM Trolox was used for pH 7.0, 7.4 and 9.0, and the OSS solution consisting of 2 mg/ml glucose oxidase, 2800 U/ml catalase, 4 mM trolox and 0.8% glucose was used for pH 5.5 and 6.5. While the Cy3 fluorophore was continuously excited using a 532 nm laser, fluorescence emission from both Cy3 and Cy5 fluorophores was simultaneously recorded for the green and red channels (512 × 256 pixels) by an EMCCD camera (iXON 897, Andor) at 100 ms time resolution using a custom-built prism-based total internal reflection fluorescence (pTIRF) microscope (56). Please refer to Single Molecule Instrumentation section in the Supplementary Data for instrumentation details. To confirm the presence of an active FRET pair, a 639 nm red laser was turned on toward the end of the movies. All single-molecule experiments were performed at room temperature (23°C).

Single-molecule data analysis

Acquired movies from the single-molecule experiments were processed using IDL and MatLab scripts from the smFRET data acquisition and analysis package available from the Ha Lab (https://cplc.illinois.edu/software/). Briefly, the single-molecule intensity traces generated by these scripts were manually selected for subsequent analysis based on the following features: (i) single-step photobleaching; (ii) total fluorescence of Cy3 and Cy5 exceeding 200 counts per frame and (iii) evidence of both Cy3 and Cy5 signals. The intensity–time traces exhibiting one-step photobleaching of each Cy3 and Cy5 fluorophores represent single molecules, and thus we analyzed only those molecules. The FRET efficiency (E_{FRET}) was calculated using a well-established equation as:

$$E_{FRET} = \frac{I_A}{I_D + I_A} \quad (1)$$

Where I_A and I_D stand for the background-corrected fluorescence intensities of acceptor and donor, respectively (57–59). The inter-dye distance (R) was then calculated using the following equation:

$$E_{FRET} = \frac{1}{1 + \left(\frac{R}{R_0}\right)^6} \quad (2)$$

Where R is the inter-dye distance and R_0 is the inter-dye distance at 50% E_{FRET}. The R_0 value used for the Cy3/Cy5 pair is 5.4 nm (58,60,61).

The smFRET histograms were prepared after combining the single-molecule data of several molecules (identified as N in the histograms) for the first 10–40 s observation time depending on the movies. The histograms were acquired after binning the raw data to 0.05 FRET window and fitted with Gaussian function to determine the mean FRET levels of visually apparent populations in Origin 2017.

Hidden markov model (HMM) analysis of dynamic FRET traces

Hidden markov model (HMM) analysis was performed on the dynamic traces observed at pH 6.5 using HaMMy (62,63) to calculate the rate of transitions between the FRET levels to determine the interconversion rates of the various conformers (fully folded, partially folded and fully unfolded states).

Nanopore construction and data analysis

Nanopore data were collected on a horizontal bilayer membrane apparatus described previously (64). Briefly, a DPhy:PC bilpid membrane is formed via the painting method over a 50 μm hole preformed in a 20 μm thick Teflon partition (Eastern Scientific LLC). A single α-hemolysin channel is inserted into the membrane and DNA is either ejected near the hole with a prefabricated micropipette tip or premixed in the buffer solution in the top chamber. An applied transmembrane potential (typically 100 mV) drives DNA into the nanopore and current is measured with an Axopatch 200B headstage amplifier (Molecular Devices). The signal is digitized (Digidata 1440, Molecular Devices) at 50 kHz and filtered with a lowpass four-pole Bessel filter with a 3dB frequency of 10 kHz. The data are processed with either homemade software (Labview 11) or packaged software (IGOR 6) and details on the threshold algorithm are described elsewhere (65). To calculate the percent translocations, the blockade events were deemed to be translocations if they exhibited a transient deep blockade or a transient shallow blockade followed by a transient deep blockade. In other words, a current blockade that led to a deep blockade from the open state or from a partially blocked state was treated as a translocation event. The fact that a lower percentage of events yielded translocations at pH 6.5 as compared to pH 8.0 indicates that the DNA was folding into a partially folded or intermediate structure at pH 6.5 while the 'infinite' blockade at pH 5.5 indicates the formation of the i-motif structure.

RESULTS AND DISCUSSION

i-motif within DNA duplexes and nanocircles—design and assembly

A number of previous studies have reported that the DNA duplexes as well as mini/nanocircles made up of short oligonucleotides can be used to mimic *in vivo* topological properties of nucleic acids (38,66,67). In this

study, we investigated the stabilities and dynamics of i-motif forming sequence from human telomere (hTel, 5′-CCCTAACCCTAACCCTAACCC) that is either flanked by a dsDNA or sandwiched between two dsDNA segments. The designed DNA constructs contain the hTel sequence either at the terminal position of a DNA duplex (*T−i-motif*), embedded between two DNA duplexes (*i-duplex*), or within DNA nanocircles (*i-Cir96* and *i-Cir75*, where 96 and 75 represent the total number of base-pairs (bp) of the double-stranded portion of the nanocircles). Additionally, in all of these assemblies, the hTel sequence was flanked by a single thymine (T) nucleotide on both sides of the sequence to allow some flexibility on i-motif folding. The DNA nanoassemblies (Figure 1A) were prepared by thermal annealing of an equimolar mixture of corresponding single-stranded DNA oligonucleotides (see Supplementary Table S1 for the sequence details and Supplementary Table S2 for the annealing protocol) in 1 × TAE buffer containing 10 mM Mg^{2+} (1 × TAE-Mg, pH 7.4). Native polyacrylamide gel electrophoresis showed a slower mobility of nanostructures with their increasing molecular weight, suggesting a successful formation of the nanoassemblies (Supplementary Figure S1).

Single-molecule setup and characterization

To determine the conformation and folding/unfolding kinetics of the hTel i-motif using smFRET, a donor (Cy3) and an acceptor (Cy5) fluorophore was incorporated into the DNA nanoassemblies as shown in Figure 1A (see Supplementary Table S1 for sequence details). The detailed microscope setup as well as the flow cell design, assembly and surface functionalization are described in the Supplementary Data (Supplementary Figure S2). In these experiments, we acquired FRET movies by monitoring the fluorescence emissions of both Cy3 and Cy5 fluorophores while the molecules are excited by a green laser (532 nm). Since the hTel sequence is known to fold into an i-motif structure at acidic pH and unfold into a random coil conformation at basic pH (68) (Figure 1B), we monitored this behavior at various pH. Depending on the conformations of the hTel sequence, different inter-dye distances (R) are expected, leading to different FRET efficiencies, E_{FRET} (Equations 1 and 2). Such a design is optimal for determining conformations and dynamics of nanoscale (<10 nm) nucleic acid structures using smFRET (69–72). We also employed another single-molecule approach called resistive-pulse nanopore sensing to characterize the hTel i-motif at various pH (Figure 1C). Nanopore sensing captures faster dynamics that are not easily accessed by smFRET due to averaging (typically ∼50–100 ms in smFRET). In this regard, an α-hemolysin nanopore was prepared by embedding the protein into a lipid bilayer (see 'Materials and Methods' section), which gives a well-defined nanohole through which current can flow when potential is applied across the opening (Figure 1C). The nanocavity (∼3.0 nm) in the α-hemolysin (73) is optimal to trap hTel i-motif (∼3.1 nm × 2.0 nm) (68) without letting it translocate, giving an opportunity to interrogate its pH-dependent response.

pH-dependent folding of the hTel i-motif

Next, we systematically studied the pH-dependent folding/unfolding behavior of i-motif in various DNA nanoassemblies (Figure 2). The typical raw intensity–time traces and corresponding FRET traces are shown in Figure 3A and Supplementary Figure S3. The smFRET histograms acquired for these nanoassemblies at various pH are shown in Figure 2. When compared, the smFRET histograms show only one population for each nanoassembly (*T−i-motif*, *i-duplex*, *i-Cir96* and *i-Cir75*) at pH 5.5 (Figure 2). The consistently high mean E_{FRET} (∼0.80) at pH 5.5 demonstrates that regardless of the DNA topological environments the hTel sequence folds into an i-motif structure at this pH. Interestingly, a slightly lower mean E_{FRET} value (∼0.75 instead of ∼0.85) was observed for *i-Cir96* and *i-Cir75*. These results indicated that, unlike in linear constructs, the hTel sequence experiences an outward tension in circular constructs resulting in an extended conformation of thymine spacers protruding from the core of the fold that are used to provide flexibility on i-motif folding (Supplementary Figure S4, left panel). The control experiment without the thymine spacers in *i-Cir75* at pH 5.5 yielded a major population (∼66%) with an E_{FRET} value of ∼0.92 along with a mid-FRET (∼16%) and low-FRET (∼18%) states (Supplementary Figure S5). While the slight increase in the E_{FRET} value without the thymine spacers (E_{FRET} = ∼0.75 in the presence of spacers to ∼0.92 without spacers) is expected due to increase in donor/acceptor proximity, the emergence of the mid- and low-FRET states suggest that the thymine spacers indeed help alleviate the constraint allowing the i-motif folding. The same nanoassembly containing a randomized hTel sequence with the same base content (Supplementary Table S1) showed a broad distribution of E_{FRET} that was significantly shifted to a lower FRET region than for i-motif, suggesting that the randomized sequence was incapable of forming an i-motif structure (Supplementary Figure S6A). CD experiments of the randomized hTel sequence did not show any signature for i-motif (Supplementary Figure S6B), suggesting that the broad E_{FRET} observed in the single-molecule experiment is possibly due to non-i-motif interactions between protonated cytosines at pH 5.5.

Next, we examined all of the nanoassemblies at pH 6.5 (Figure 2). Interestingly, we observed new FRET states at ∼0.6 and ∼0.2 in addition to ∼0.8 for *T-i-motif* and *i-duplex*. These results suggest that, in addition to fully folded (∼0.8) and fully unfolded (∼0.2) states, the hTel sequence exhibits at least one partially folded state. Our assessment of a partially folded state (E_{FRET} = ∼0.6) is consistent with the formation of a triplex-like structure (discussed in detail later) as reported previously in other i-motif forming sequences (Supplementary Figure S4 and Supplementary Note 1) (5,74). While *T-i-motif* and *i-duplex* show approximately similar E_{FRET} distributions, the high FRET population (∼0.8) was absent in *i-Cir96* and there was an emergence of a new population with a mean E_{FRET} value of ∼0.4. These results suggest that the hTel i-motif experiences an outward strain in *i-Cir96* and thus destabilizes the folding. We attributed that the decrease in the mean E_{FRET} value from 0.6 in *i-duplex* to 0.4 in *i-Cir96* is due to the

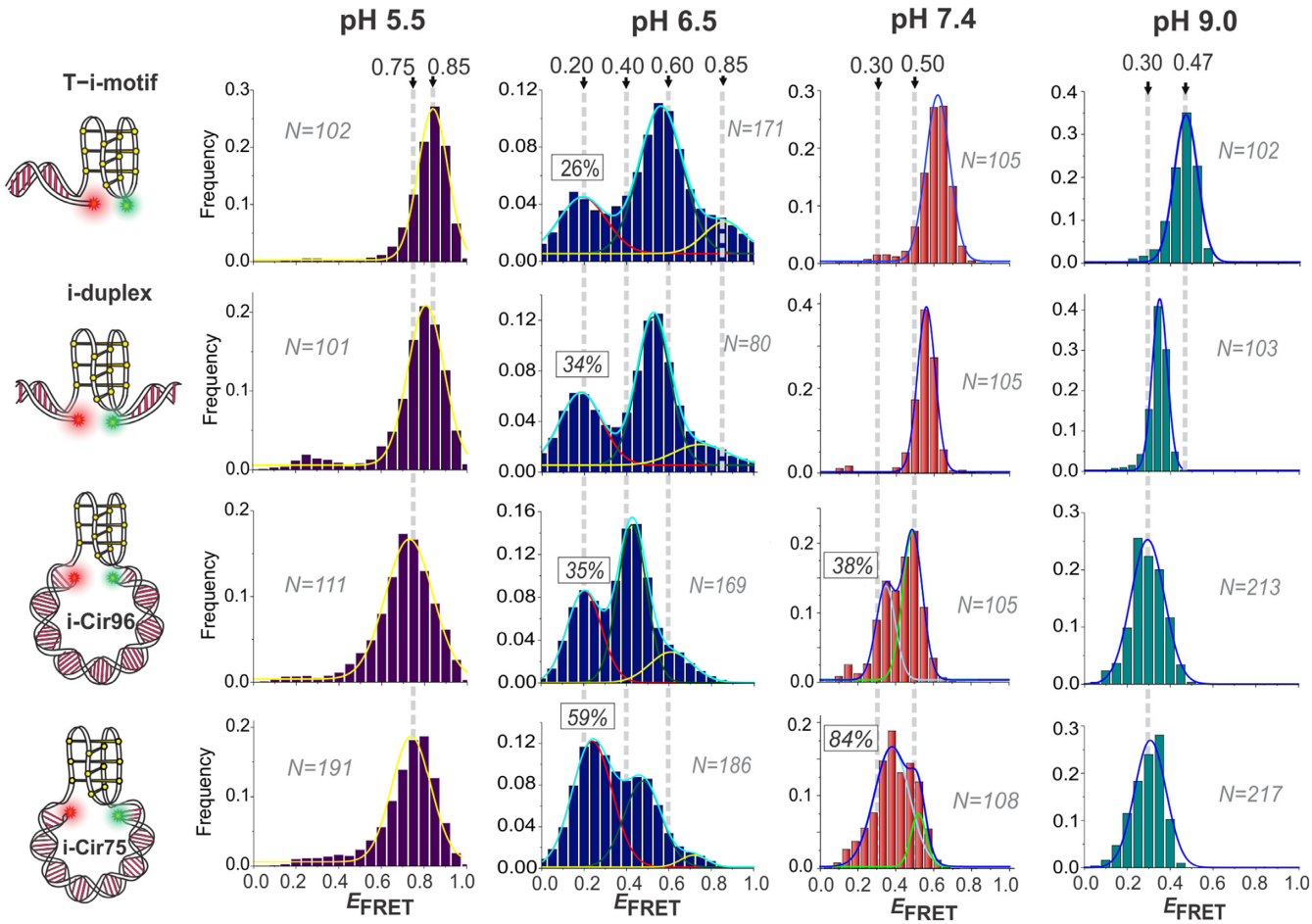

Figure 2. Single-molecule analysis of the hTel i-motif under different topological environments and pH. smFRET histograms of *T-i-motif* (first row), *i-duplex* (second row), *i-Cir96* (third row) and *i-Cir75* (fourth row). All histograms were fitted with one-, two- or three-peak Gaussian functions (depicted by curves) to determine the mean E_{FRET} and their corresponding populations. Since the *y*-axis scale varies in some histograms, we have identified the percentage population of the unfolded state at pH 6.5 and 7.4 for an easy comparison when multiple populations were observed. The mean E_{FRET} are identified by the vertical dotted lines. The *N* values depict the number of single-molecule traces in each histogram. All measurements were performed at room temperature (23°C).

extended conformation of thymine spacers in *i-Cir96*. This assignment is self-consistent with our observation that the *i-Cir96* exhibited a slightly lower E_{FRET} (∼0.75) than that of *T-i-motif* and *i-duplex* (∼0.8) at pH 5.5. We also performed circular dichroism (CD) experiments of hTel 23-mer oligonucleotide and other control sequences at various pH (Supplementary Figure S7). The CD experiments show general agreement with our smFRET results that the i-motif is formed at acidic pH (characteristic peak at ∼285–288 nm and trough at ∼260 nm) (22). The CD spectrum of a truncated sequence with three intact C-rich stretches also supported the formation of a partially folded state at acidic pH (Supplementary Figure S7C). However, CD being an ensemble measurement, it was not possible to extract the detailed insight into the dynamic behavior of the i-motif and partially folded state.

To unequivocally determine that the DNA nanocircles indeed impose a topological strain on i-motif, we further decreased the size of the nanocircles from 96 bp (*i-Cir96*) to 75 bp (*i-Cir75*). The topological strain is expected to increase with decrease in the size of nanocircles. Interestingly, *i-Cir75* indeed showed further decrease in the mid-FRET (∼0.4) population and increase in the low-FRET (∼0.2) population. When compared, the low-FRET (∼0.2) population is monotonically increased from *T-i-motif* (26%) → *i-duplex* (34%) → *i-Cir96* (35%) → *i-Cir75* (59%) confirming: (i) the existence of an outward strain in nanocircles and (ii) the strain significantly hinders folding. Further, having a small single-stranded region within *i-Cir96* (created by truncation of the middle strand by 10 nucleotides), we observed a slight shift in the mid-FRET population toward higher E_{FRET} state at pH 6.5 (Supplementary Figure S8). This result corroborates our conclusion that the nanocircles exhibit topological constraint on i-motif.

We then analyzed these nanoassemblies at pH 7.4 and 9.0. While all the nanoassemblies show a mid-FRET state at pH 7.4 (Figure 2 and Supplementary Figure S3), only a fully unfolded state with a low E_{FRET} value (∼0.3) was observed at pH 9.0, except for *T-i-motif*. We reason that, unlike in other nanoassemblies, the hTel sequence in *T-i-motif* adopts a random coil conformation due to its free end, leading to a mid-FRET state (∼0.5) (75). Consistent

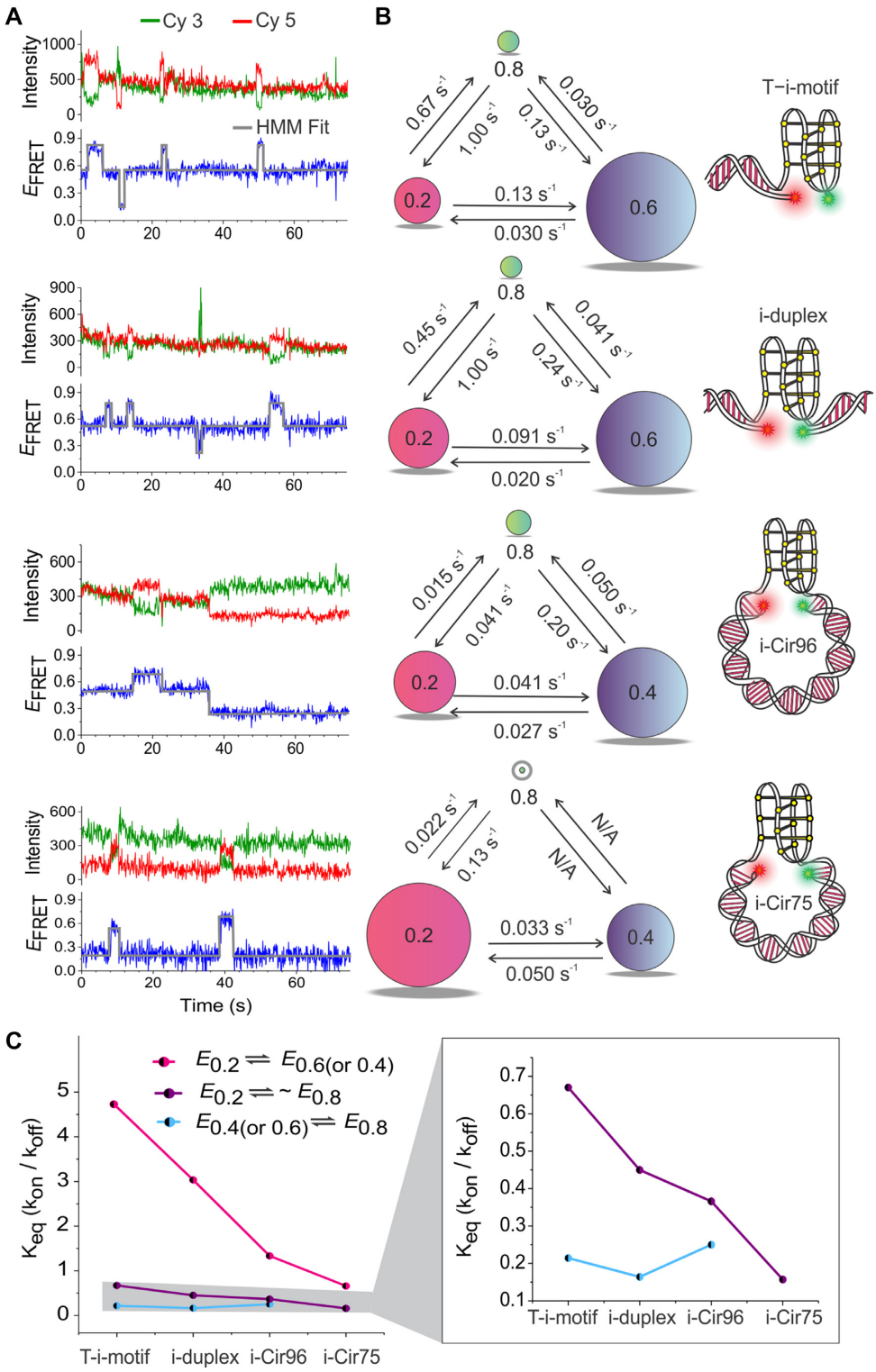

Figure 3. Conformational dynamics of i-motif at pH 6.5. (**A**) Typical smFRET-time traces for each type of DNA assembly (collected at the time resolution of 100 ms). Top panel: raw intensity–time traces for Cy3 (green) and Cy5 (red). Bottom panel: FRET traces calculated from the raw intensity traces shown in the top panel. (**B**) Kinetic analysis of i-motif. The relative populations of FRET states (labeled inside the sphere) for the given construct are reflected by the size of spheres. Arrows represent the directions of transitions. The transition rates are directly labeled by the arrows. These rates were determined from more than 1000 transitions for each nanoassembly (2309, 1226, 1095 and 1126 transitions for *T-i-motif*, *i-duplex*, *i-Cir96* and *i-Cir75*, respectively). The high FRET state in *i-Cir75* is very small (3%); therefore, the sphere representing this population is circled for the visualization purpose. (**C**) The equilibrium transition rate (K_{eq}), defined as k_{on}/k_{off}, of various FRET transitions determined by Hidden Markov model (HMM) analysis of the FRET traces, where k_{on} and k_{off} represent the folding and unfolding rate, respectively. Transitions with $K_{eq} > 1$ represent preferred folding whereas the transitions with $K_{eq} < 1$ represent preferred unfolding. N/A = not applicable, due to insufficient transitions making the kinetic data not reliable.

with CD (Supplementary Figure S7D), our control experiment in the presence of complementary G-rich strand at pH 9.0 using *i-duplex* showed a slightly lower mean E_{FRET} value of ∼0.2 (compared to ∼0.3 without G-rich strand) suggesting the formation of dsDNA (Supplementary Figure S9). The formation of the partially folded state at pH 7.4 is supported by the fact that the E_{FRET} at this pH was consistently higher than for the unfolded state at either pH 6.5 or 9.0 (Figure 2) and for randomized hTel at pH 7.4 (Supplementary Figure S10). It is possible that the partially folded state observed here was stabilized by the topological constraint caused by flanking DNA duplexes or nanocircles, but it needs further investigation. In addition to the partially folded states (E_{FRET} = ∼0.4 and ∼0.6), a fully unfolded state (E_{FRET} = ∼0.3) is also observed in the circular constructs (*i-Cir96* and *i-Cir75*) (Figure 2), showing that there is an outward strain in the nanocircles. The increased population of the fully unfolded state in *i-Cir75* compared to that of *i-Cir96* further confirms the higher topological strain experienced in *i-Cir75*. Overall, these results demonstrated that the folding and conformational dynamics of hTel sequence are significantly affected by the biomimetic topological environments. Interestingly, we also observed that the fully unfolded state of hTel sequence at pH 6.5 consistently exhibits a slightly lower E_{FRET} compared to that at basic pH (∼0.2 at pH 6.5 versus ∼0.3 at pH 7.4 and 9.0). Previous studies show that the effect of pH on fluorescence emission of symmetrical cyanine dyes (like Cy3 and Cy5 used in this study) is minimal (76); therefore, slightly higher E_{FRET} observed for the unfolded state at basic pH indicates that the pH has an effect on the hTel conformation when unfolded, which can be a subject of future study. In addition, the experiment performed in the presence of complementary G-rich sequence (1 μM) using *i-duplex* at near neutral pH (pH 6.5) showed no evidence of folding (Supplementary Figure S9), suggesting that the G-rich strand obviates the formation of i-motif at this pH. However, this experiment does not rule out the formation of i-motif inside cells where DNA experiences other factors including crowding (14–16).

Conformational dynamics of hTel i-motif

While the FRET traces at pH 5.5, 7.4 and 9.0 were static (Supplementary Figure S3), visually distinct low-, mid- and high-FRET states (Figure 3A) were observed at pH 6.5, suggesting an equilibrium switching between fully unfolded, partially folded and fully folded states respectively at this pH. Partially folded intermediate states of i-motif forming sequences have been reported in the literature (5,74,77,78). The typical traces for each nanoassembly are presented in Figure 3A. The switching rates obtained from the well-known HMM analysis (62,63) (see 'Materials and Methods' section and Supplementary Figure S11) are summarized in Figure 3B. The kinetic analysis of these data revealed some interesting insights of the behavior of hTel sequence. The switching rates of various species were different from one another in different nanoassemblies ranging from 0.01 to 1.00 s^{-1}. The lifetimes for the partially folded and fully folded states (overall from all the linear and circular constructs) were calculated to be 31 ± 11 s and 6 ± 2 s, respectively, at pH 6.5. The lifetime for the hTel i-motif determined here is in good agreement with the reported lifetime of ∼3 s at neutral pH (longer lifetime is expected at pH 6.5 compared to neutral pH) (55). It is possible that the conformational switching observed here is due to the dynamic proton exchange between the i-motif and solution (79). This result suggests that the local change in pH inside cells could trigger transient formation of i-motif. Further, the analysis of equilibrium constant K_{eq}, defined as k_{on}/k_{off} where k_{on} represents the folding and k_{off} represents the unfolding rate, showed that the i-motif is only transiently formed in non-circular constructs. The downward trend of K_{eq} from fully unfolded (E_{FRET} = ∼0.3) to partially (E_{FRET} = ∼0.4 or 0.6) or fully folded (E_{FRET} = ∼0.8) states going from *T-i-motif* → *i-duplex* → *i-Cir96* → *i-Cir75* (Figure 3C) suggests that the folding is hindered when both ends of the hTel sequence are flanked by DNA duplexes. This effect is more pronounced in nanocircles than in linear constructs (*T-i-motif* and *i-duplex*), suggesting that the topological strain is dominant in nanocircles. In addition, the mean lifetime of the partially folded state in the circular constructs (26 s) is shorter than in linear constructs (35 s), suggesting that the hTel sequence indeed experiences topological strain in circular constructs. These analyses corroborate our conclusion in Figure 2 that the folding of hTel i-motif is restricted in the circular constructs. Furthermore, the switching between the fully folded and partially folded (relaxed E_{FRET} = ∼0.6 and extended E_{FRET} = ∼0.4) states showed similar but low K_{eq} values suggesting that the extended conformation is preferred except in *T-i-motif* at pH 6.5 (Figure 3C). Similar analysis was not possible in *i-Cir75* due to rare transitions between those FRET states.

The smFRET experiments at pH 7.4 showed a mid-FRET state in all of the nanoassemblies (Figure 2). This observation was surprising because at least two possible partially folded states, each of which is formed by three of the four C-rich stretches (Supplementary Note S1), are expected (5,74). However, both of these states will provide similar E_{FRET} values in the FRET experiments making it impossible to resolve any conformational switching. Also, the smFRET experiments at our time resolution of 100 ms cannot rule out the possible fast dynamics between the partially folded and unfolded states. To further investigate this dynamical behavior of hTel sequence, we turned to nanopore experiments where we can measure thousands of single-molecule events in short periods to assess the relative abundance of fully unfolded, partially folded and fully folded states as a function of solution pH and applied transmembrane potential. When the plain i-motif sequence with no overhangs was analyzed by an α-hemolysin (α-HL) nanopore at various pH (Figure 4), we found a general agreement with the FRET data and supporting evidence of the existence of partially folded states at near neutral pH (pH 6.5).

The current versus time (*i–t*) traces show pH-dependent blockades when the i-motif is present in the α-HL nanocavity. At pH 8.0 and 6.5, the DNA molecules yielded short downward spikes in the current (Figure 4A and B) and a zoomed in view of these spikes showed three distinct blockades (Figure 4C) that were different from the long-lived blockades at pH 5.5 (Figure 4D). Two of the three yielded deep current blocks, which correspond to translocations

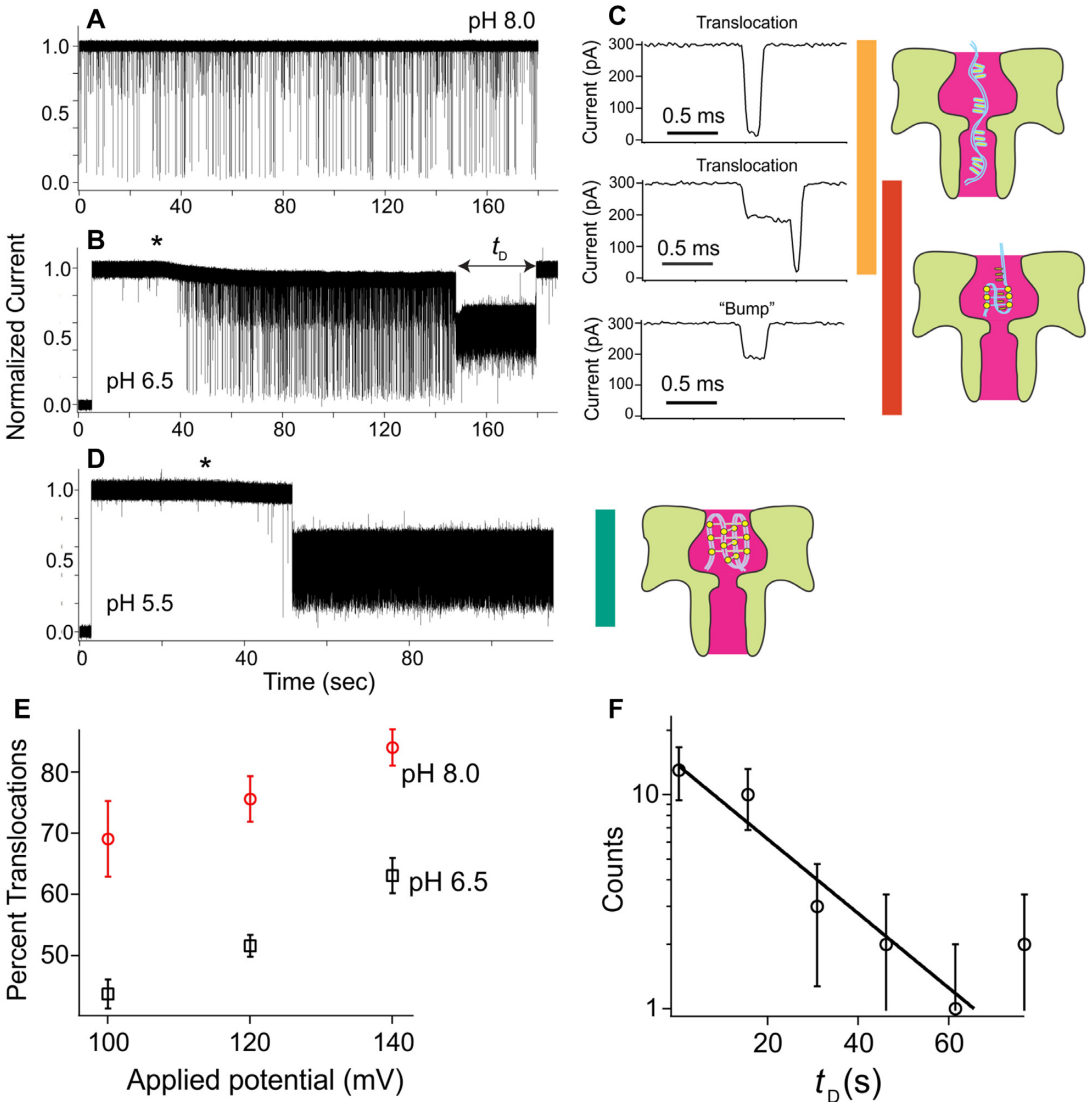

Figure 4. Nanopore analysis of 21-mer hTel sequence without overhangs as a function of pH and voltage. (**A** and **B**) At higher pH (8.0, 6.5), the DNA enters and exits the pore rapidly giving rise to short-lived, downward current spikes. (**C**) These short spikes exhibit three distinct current signatures. Deeper current blockades correspond to translocation through the pore while shallow blockades correspond to short-lived 'bumping' events. While it is not possible to assign a DNA folding state to each short-lived blockade, our data suggest that partially folded DNA will more likely yield bumping events without translocation through the pore. This can be used to observe subtle changes in the DNA folding state as a function of pH. (**D**) At pH 5.5, the short blockades are eliminated, and only long-lived ('permanent') and noisy current states are observed. This is consistent with fully folded i-motif structures entering the pore for extended periods. This indicates a clear structural transition between pH 6.5 and 5.5. (**E**) Analysis of the short-lived blockades shows a gradual transition between the fully unfolded state and the partially folded state as evidenced by the higher percentage of translocation events seen between pH 8 (circles) and 6.5 (squares). (**F**) The duration of the long-lived blockades at pH 6.5 is exponentially distributed with a mean time, $t_D = (25 \pm 6)$ s, which is consistent with the lifetime seen in the FRET data in Figure 3. The asterisks in (B) and (D) correspond to the start times when the DNA was injected in the vicinity of the pore from a pre-positioned microcapillary tip. Except in panel (E), all measurements were taken in 3 M KCl under a 100 mV applied transmembrane potential at room temperature (23°C).

through the pore (Figure 4C) and the third results from a DNA molecule 'bumping' into the pore for a short time and exiting the pore from the same side it entered. These bumping events could occur from unfolded DNA entering and exiting the pore on the same side or from partially folded DNA that does not translocate through the pore. This second scenario is supported by the data in Figure 4E that show the number of bumping events is higher at pH 6.5. This is consistent with our hypothesis that lowering the pH yields intermediate or partially folded states that are more likely to 'bump' off the pore rather than translocate through. The two deep blockade types most likely resulted from either fully unfolded or partially folded DNA states. However, it is not possible to distinguish the DNA states from these types of blockades. In both cases, the single-stranded portion of the DNA enters the pore and is pulled through under a sufficient transmembrane potential. In addition to the short-lived blockades at pH 6.5, we also observed longer lived blockades that most likely correspond to partially folded states. Figure 4F shows the long-lived

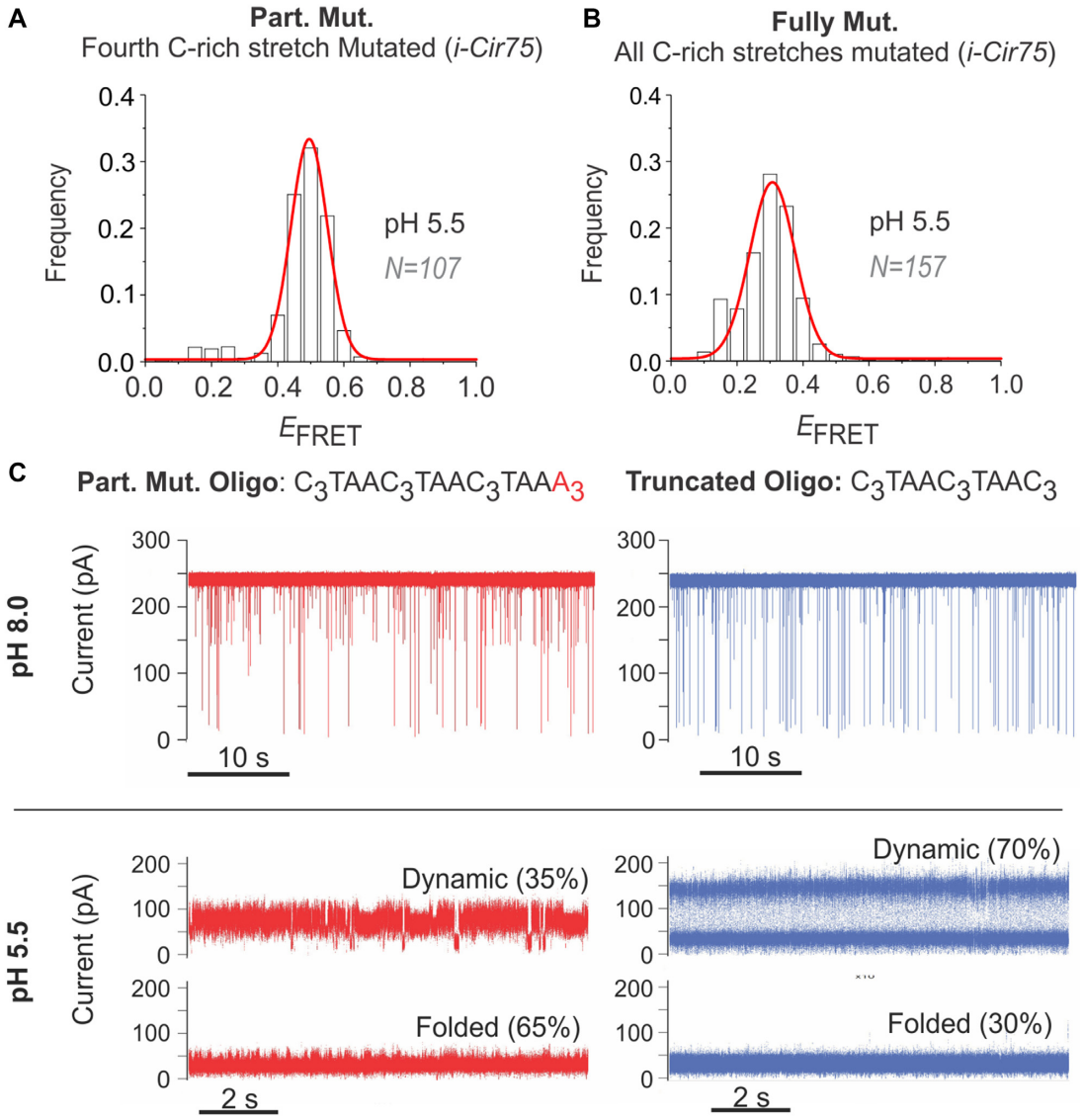

Figure 5. Mutation/deletion analysis of hTel sequence. (**A**) smFRET histogram after modifying the fourth C-rich stretch (cytosine to adenine, 'Part. Mut.') at pH 5.5. (**B**) smFRET histogram of fully mutated ('Fully Mut.') sequence at pH 5.5. Both of these experiments were performed using *i-Cir75* in the presence of thymine spacers. (**C**) Nanopore analyses of the 21-mer Part. Mut. (left) and truncated sequence (with only three intact C-rich stretches, right) at pH 8.0 (top) and 5.5 (bottom). Both of these sequences demonstrate the formation of a stable structure at acidic pH. Note the different time and current scales at acidic pH. The acidic pH current traces each correspond to a single trapped molecule while the fluctuations at pH 8.0 result from a large number of short-lived events. Data shown here were collected under 100 mV applied transmembrane potential in a 3 M KCl electrolyte solution.

blockade time distribution with a mean blockade time of 25 s, which is consistent with the lifetime of the partially folded state in the FRET data from Figure 3. Finally, Figure 4D shows that lowering the pH to 5.5 eliminates the short-lived blockades and only produces the long-lived blockades. These blockades reside permanently in the pore so no lifetime measurement was possible. At this pH, it appears that the fully folded state is stable as seen in the smFRET data (Figure 2, pH 7.4). The nanopore data in Figure 4 support the smFRET results that show a partially folded state dominates at near neutral pH (pH 6.5 and 7.4, Figure 2 and Supplementary Figure S4), whereas the i-motif is predominant at pH 5.5 (24).

We further examined the formation of partially folded states by changing the fourth C-rich stretch of the hTel sequence to adenines (Partially Mutated, abbreviated as 'Part. Mut': $C_3TAAC_3TAAC_3TAAA_3$). In the smFRET experiment using *i-Cir75*, we observed a mean E_{FRET} state of ~0.49 at pH 5.5 (Figure 5A), which is consistent with the partially folded state observed for the same nanoassembly at pH 6.5 (Figure 2). Additionally, mutation of all of the C-rich stretches of the hTel sequence provided an expected mean E_{FRET} of ~0.3 (Figure 5B) at pH 5.5. This observation was consistent with the ~0.3 E_{FRET} observed for the hTel sequence at various pH for the fully unfolded state. To unequivocally examine the formation of the partially folded state, we ran nanopore experiments for the

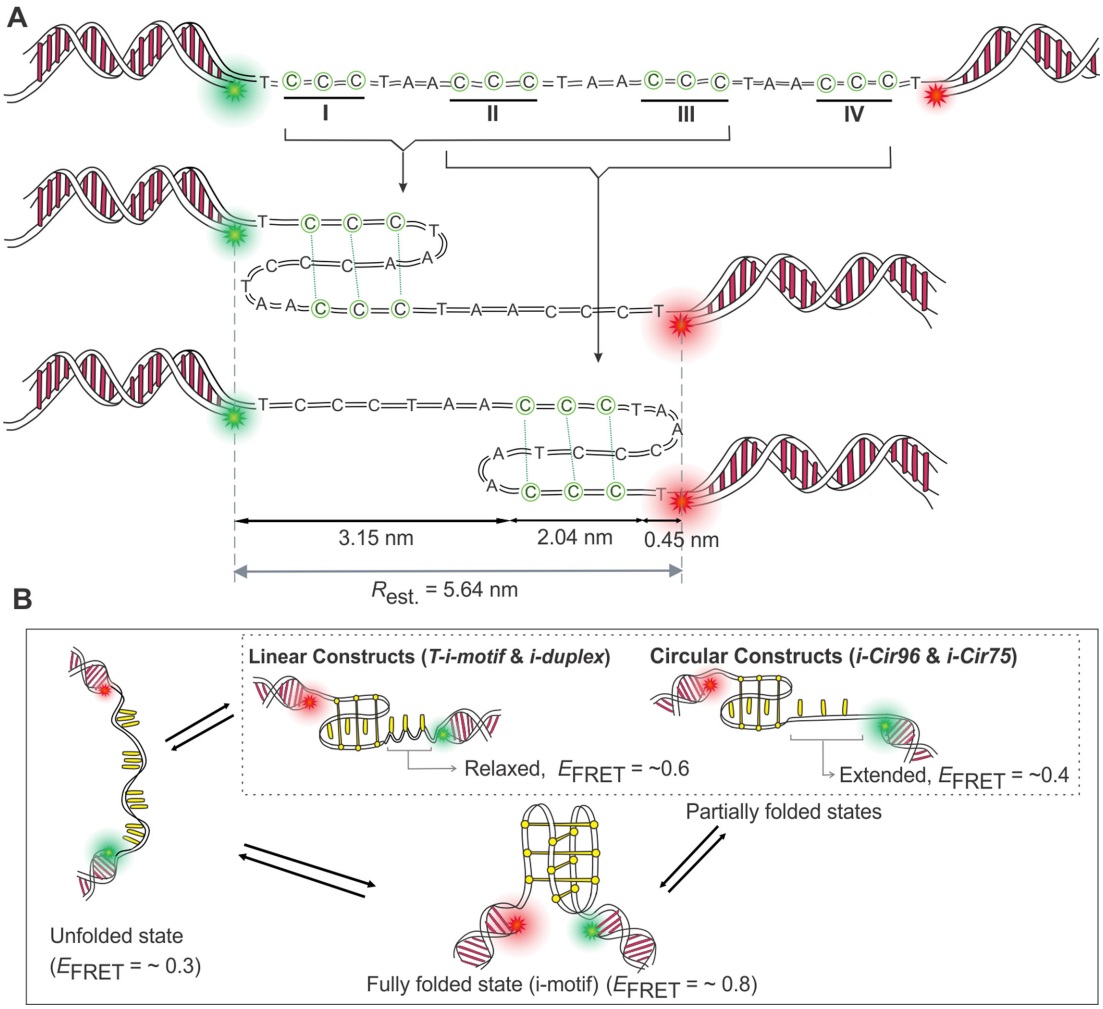

Figure 6. Model of i-motif dynamics. (**A**) Schematic illustration of two plausible ways of forming partially folded states. The four cytosine(C)-rich stretches in hTel are highlighted (I–IV). Two partially folded states—either involving the first three (I, II and III; middle panel) or the last three (II, III and IV; bottom panel) C-rich stretches, each providing identical FRET efficiency (E_{FRET}) due to same inter-dye distance (R). The cytosines involved in the CH^+• C formation are circled. The inter-dye distance was estimated (R_{est}) assuming the contour length of nucleotide to be 0.45 nm and the dimension of triplex-like structure to be 2.04 nm (PDB: 1ELN). See Supplementary Note S1 for the details. (**B**) Summary of the conformational transitions observed in single-molecule analysis of hTel sequence. The fully unfolded state, the partially folded states and fully folded i-motif are shown with their respective FRET efficiencies, E_{FRET}. The E_{FRET} of the partially folded states at relaxed (linear constructs) and extended state (circular constructs) are highlighted.

Part. Mut. and Truncated (fourth C-rich tract deleted) sequences (Figure 5C). Both of these sequences at pH 8.0 exhibited high, open-pore, current with transient dips in the *i–t* curves, demonstrating quick translocations (lack of folding) of the oligonucleotides (Figure 5C, top panel).

However, the same sequences at pH 5.5 show evidence of folding as they lead to two types of long-lived blockade states (i) dynamic two-state fluctuations and (ii) single state. For the 'Part. Mut.' sequence, a majority of molecules (~65%) show long-lived deep blockades and some two-state fluctuations (35%). In contrast, the majority of molecules (70%) show two-state fluctuations for the truncated sequence. These observations strongly suggest that both the Part. Mut. and Truncated versions of the hTel sequences assume some sort of folded structures (otherwise they would translocate as observed in pH 8.0). For the higher fraction of long-lived deep blockades in Part. Mut. sequence, it is possible that the single-stranded overhang (polyA tail) at the 3′-end gets inserted into the nanopore blocking the current. Since such polyA tail was absent in the truncated sequence, we surmised that the two-state fluctuations are due to tumbling of the partially folded structure (as it is not strongly pulled as with the polyA tail) inside the nanopore cavity.

Overall, both smFRET and nanopore data demonstrated that the hTel sequence exhibits a fully unfolded state at basic pH, fully folded state at pH 5.5 and partially folded states at pH 6.5 (Figure 6B). In linear constructs, where the topological restriction is either absent or minimal, the i-motif forming sequence assumes a relaxed, partially folded state (E_{FRET} = ~0.6). However, an extended form of the partially folded state (E_{FRET} = ~0.4) is predominant in circular constructs at near neutral pH (pH 6.5 and 7.4). Our results thereby provide a more detailed understanding on the folding behavior of hTel sequence under biologically relevant microenvironments.

CONCLUSIONS

We have systematically studied the folding and conformational dynamics of the hTel C-rich sequence at the single-molecule level, directly revealing the effect of topological constraint/strain from flanking dsDNA and DNA nanocircles. Regardless of the topological constraint, we show that the hTel sequence adopts a fully folded state at pH 5.5 and a fully unfolded state at high pH (8.0 and 9.0). However, the sequence undergoes conformational dynamics among fully unfolded, partially folded and i-motif structures at pH 6.5 on a topological environment-dependent manner. Using nanopore analysis, we determined the relative abundance of fully unfolded, partially folded and fully folded states as a function of pH and applied transmembrane potential. Nanopore analysis of the plain i-motif sequence with no overhangs at pH 6.5 provided evidence for a partially folded state that is consistent with the smFRET and CD data. Given that the nanocircle framework provides conditions closer to cellular environments, our approach has a high potential to be used in studying the interaction of small molecule ligands and proteins such as transcription factors, revealing biologically relevant information. In the future, the study can be performed on ligated nanocircles to explore the effects of increased rigidity on the i-motif stability and conformational dynamics. Furthermore, the molecular approaches developed here for studying i-motif are simple and can be easily adopted to study other nucleic acids structures and these nanoassemblies may find applications in studying proteins that interact with cytosine-rich sequences.

SUPPLEMENTARY DATA

Supplementary Data are available at NAR Online.

ACKNOWLEDGEMENTS

S.D. acknowledges the Farrell lab and the Department of Chemistry, VCU for the CD instrument.

FUNDING

Virginia Commonwealth University (VCU Startup Grant) (to S.D.); VCU SEED award (to J.E.R.). Funding for open access charge: Virginia Commonwealth University.
Conflict of interest statement. None declared.

REFERENCES

1. Gehring,K., Leroy,J.-L. and Guéron,M. (1993) A tetrameric DNA structure with protonated cytosine-cytosine base pairs. *Nature*, **363**, 561–565.
2. Mergny,J.-L., Lacroix,L., Han,X., Leroy,J.-L. and Helene,C. (1995) Intramolecular folding of pyrimidine oligodeoxynucleotides into an i-DNA Motif. *J. Am. Chem. Soc.*, **117**, 8887–8898.
3. Mir,B., Serrano,I., Buitrago,D., Orozco,M., Escaja,N. and González,C. (2017) Prevalent sequences in the human genome can form mini i-motif structures at physiological pH. *J. Am. Chem. Soc.*, **139**, 13985–13988.
4. Wright,E.P., Huppert,J.L. and Waller,Zoë A E. (2017) Identification of multiple genomic DNA sequences which form i-motif structures at neutral pH. *Nucleic Acids Res.*, **45**, 2951–2959.
5. Dhakal,S., Schonhoft,J.D., Koirala,D., Yu,Z., Basu,S. and Mao,H. (2010) Coexistence of an ILPR i-Motif and a partially folded structure with comparable mechanical stability revealed at the single-molecule level. *J. Am. Chem. Soc.*, **132**, 8991–8997.
6. Niu,K., Zhang,X., Deng,H., Wu,F., Ren,Y., Xiang,H., Zheng,S., Liu,L., Huang,L., Zeng,B. *et al.* (2018) BmILF and i-motif structure are involved in transcriptional regulation of BmPOUM2 in Bombyx mori. *Nucleic Acids Res.*, **46**, 1710–1723.
7. Kang,H.-J., Kendrick,S., Hecht,S.M. and Hurley,L.H. (2014) The Transcriptional complex between the BCL2 i-Motif and hnRNP LL Is a molecular switch for control of gene expression that can be modulated by small molecules. *J. Am. Chem. Soc.*, **136**, 4172–4185.
8. Guo,K., Pourpak,A., Beetz-Rogers,K., Gokhale,V., Sun,D. and Hurley,L.H. (2007) Formation of pseudo-symmetrical G-quadruplex and i-motif structures in the proximal promoter region of the RET oncogene. *J. Am. Chem. Soc.*, **129**, 10220–10228.
9. Balasubramanian,S., Hurley,L.H. and Neidle,S. (2011) Targeting G-quadruplexes in gene promoters: a novel anticancer strategy? *Nat. Rev. Drug Discov.*, **10**, 261–275.
10. Takahashi,S., Brazier,J.A. and Sugimoto,N. (2017) Topological impact of noncanonical DNA structures on Klenow fragment of DNA polymerase. *Proc. Natl. Acad. Sci. U.S.A.*, **114**, 9605–9610.
11. Zeraati,M., Langley,D.B., Schofield,P., Moye,A.L., Rouet,R., Hughes,W.E., Bryan,T.M., Dinger,M.E. and Christ,D. (2018) I-motif DNA structures are formed in the nuclei of human cells. *Nat. Chem.*, **10**, 631–637.
12. Abou Assi,H., Garavís,M., González,C. and Damha,M.J. (2018) i-Motif DNA: structural features and significance to cell biology. *Nucleic Acids Res.*, **46**, 8038–8056.
13. Dzatko,S., Krafcikova,M., Hänsel-Hertsch,R., Fessl,T., Fiala,R., Loja,T., Krafcik,D., Mergny,J.L., Foldynova-Trantirkova,S. and Trantirek,L. (2017) Evaluation of the stability of DNA i-Motifs in the nuclei of living mammalian cells. *Angew. Chem. Int. Ed.*, **57**, 2165–2169.
14. Cui,J., Waltman,P., Le,V.H. and Lewis,E.A. (2013) The effect of molecular crowding on the stability of human c-MYC promoter sequence I-motif at neutral pH. *Molecules*, **18**, 12751–12767.
15. Rajendran,A., Nakano,S.-I. and Sugimoto,N. (2010) Molecular crowding of the cosolutes induces an intramolecular i-motif structure of triplet repeat DNA oligomers at neutral pH. *Chem. Commun.*, **46**, 1299–1301.
16. Saxena,S., Joshi,S., Shankaraswamy,J., Tyagi,S. and Kukreti,S. (2017) Magnesium and molecular crowding of the cosolutes stabilize the i-motif structure at physiological pH. *Biopolymers*, **107**, e23018.
17. Sun,D. and Hurley,L.H. (2009) The Importance of Negative Superhelicity in Inducing the Formation of G-Quadruplex and i-Motif Structures in the c-Myc Promoter: Implications for Drug Targeting and Control of Gene Expression. *J. Med. Chem.*, **52**, 2863–2874.
18. Sutherland,C., Cui,Y., Mao,H. and Hurley,L.H. (2016) A mechanosensor mechanism controls the G-quadruplex/i-Motif molecular switch in the MYC promoter NHE III1. *J. Am. Chem. Soc.*, **138**, 14138–14151.
19. Selvam,S., Koirala,D., Yu,Z. and Mao,H. (2014) Quantification of topological coupling between DNA superhelicity and G-quadruplex formation. *J. Am. Chem. Soc.*, **136**, 13967–13970.
20. Leroy,J.-L., Guéron,M., Hélène,C. and Mergny,J.-L. (1994) Intramolecular folding of a fragment of the cytosine-rich strand of telomeric DNA into an i-motif. *Nucleic Acids Res.*, **22**, 1600–1606.
21. Phan,A.T. and Mergny,J.-L. (2002) Human telomeric DNA: G-quadruplex, i-motif and Watson-Crick double helix. *Nucleic Acids Res.*, **30**, 4618–4625.
22. Manzini,G., Yathindra,N. and Xodo,L.E. (1994) Evidence for intramolecularly folded i-DNA structures in biologically relevant CCC-repeat sequences. *Nucleic Acids Res.*, **22**, 4634–4640.
23. Xu,Y. and Sugiyama,H. (2006) Formation of the G-quadruplex and i-motif structures in retinoblastoma susceptibility genes (Rb). *Nucleic Acids Res.*, **34**, 949–954.
24. Ding,Y., Fleming,A.M., He,L. and Burrows,C.J. (2015) Unfolding kinetics of the human telomere i-motif under a 10 pN force imposed by the α-hemolysin nanopore identify transient folded-state lifetimes at physiological pH. *J. Am. Chem. Soc.*, **137**, 9053–9060.
25. Choi,J. and Majima,T. (2013) Reversible conformational switching of i-Motif DNA studied by fluorescence spectroscopy. *Photochem. Photobiol.*, **89**, 513–522.
26. Dhakal,S., Yu,Z., Konik,R., Cui,Y., Koirala,D. and Mao,H. (2012) G-quadruplex and i-motif are mutually exclusive in ILPR double-stranded DNA. *Biophys. J.*, **102**, 2575–2584.

27. Benabou,S., Avino,A., Eritja,R., Gonzalez,C. and Gargallo,R. (2014) Fundamental aspects of the nucleic acid i-motif structures. *RSC Adv.*, **4**, 26956–26980.
28. Choi,J. and Majima,T. (2011) Conformational changes of non-B DNA. *Chem. Soc. Rev.*, **40**, 5893–5909.
29. König,S.L.B., Huppert,J.L., Sigel,R.K.O. and Evans,A.C. (2013) Distance-dependent duplex DNA destabilization proximal to G-quadruplex/ i -motif sequences. *Nucleic Acids Res.*, **41**, 7453–7461.
30. Assi,H.A., Harkness,V.R.W., Martin-Pintado,N., Wilds,C.J., Campos-Olivas,R., Mittermaier,A.K., González,C. and Damha,M.J. (2016) Stabilization of i-motif structures by 2′-β-fluorination of DNA. *Nucleic Acids Res.*, **44**, 4998–5009.
31. Modi,S., Swetha,M.G., Goswami,D., Gupta,G.D., Mayor,S. and Krishnan,Y. (2009) A DNA nanomachine that maps spatial and temporal pH changes inside living cells. *Nat. Nanotechnol.*, **4**, 325–330.
32. Nesterova,I.V. and Nesterov,E.E. (2014) Rational design of highly responsive pH sensors based on DNA i-Motif. *J. Am. Chem. Soc.*, **136**, 8843–8846.
33. Bath,J. and Turberfield,A.J. (2007) DNA nanomachines. *Nat. Nanotechnol.*, **2**, 275–284.
34. Surana,S., Bhat,J.M., Koushika,S.P. and Krishnan,Y. (2011) An autonomous DNA nanomachine maps spatiotemporal pH changes in a multicellular living organism. *Nat. Commun.*, **2**, 340.
35. Dong,Y., Yang,Z. and Liu,D. (2014) DNA Nanotechnology Based on i-Motif Structures. *Acc. Chem. Res.*, **47**, 1853–1860.
36. Xia,F., Guo,W., Mao,Y., Hou,X., Xue,J., Xia,H., Wang,L., Song,Y., Ji,H., Ouyang,Q. *et al.* (2008) Gating of single synthetic nanopores by proton-driven DNA molecular motors. *J. Am. Chem. Soc.*, **130**, 8345–8350.
37. Shibata,T., Fujita,Y., Ohno,H., Suzuki,Y., Hayashi,K., Komatsu,K.R., Kawasaki,S., Hidaka,K., Yonehara,S., Sugiyama,H. *et al.* (2017) Protein-driven RNA nanostructured devices that function in vitro and control mammalian cell fate. *Nat. Commun.*, **8**, 540.
38. Li,T. and Famulok,M. (2013) I-Motif-Programmed functionalization of DNA nanocircles. *J. Am. Chem. Soc.*, **135**, 1593–1599.
39. Alba,J.J., Sadurní,A. and Gargallo,R. (2016) Nucleic acid i-Motif structures in analytical chemistry. *Crit. Rev. Anal. Chem.*, **46**, 443–454.
40. Dembska,A. (2016) The analytical and biomedical potential of cytosine-rich oligonucleotides: a review. *Anal. Chim. Acta*, **930**, 1–12.
41. Sellner,S., Kocabey,S., Zhang,T., Nekolla,K., Hutten,S., Krombach,F., Liedl,T. and Rehberg,M. (2017) Dexamethasone-conjugated DNA nanotubes as anti-inflammatory agents in vivo. *Biomaterials*, **134**, 78–90.
42. McCarthy,J.G. and Heywood,S.M. (1987) A long polypyrimidine/polypurine tract induces an altered DNA conformation on the 3′ coding region of the adjacent myosin heavy chain gene. *Nucleic Acids Res.*, **15**, 8069–8085.
43. Shrestha,P., Xiao,S., Dhakal,S., Tan,Z. and Mao,H. (2014) Nascent RNA transcripts facilitate the formation of G-quadruplexes. *Nucleic Acids Res.*, **42**, 7236–7246.
44. Koirala,D., Dhakal,S., Ashbridge,B., Sannohe,Y., Rodriguez,R., Sugiyama,H., Balasubramanian,S. and Mao,H. (2011) A single-molecule platform for investigation of interactions between G-quadruplexes and small-molecule ligands. *Nat. Chem.*, **3**, 782–787.
45. Choi,J., Kim,S., Tachikawa,T., Fujitsuka,M. and Majima,T. (2011) pH-Induced Intramolecular Folding Dynamics of i-Motif DNA. *J. Am. Chem. Soc.*, **133**, 16146–16153.
46. Zhao,Y., Zeng,Z.-X., Kan,Z.-Y., Hao,Y.-H. and Tan,Z. (2005) The folding and unfolding kinetics of the i-Motif structure formed by the C-rich strand of human telomere DNA. *ChemBioChem*, **6**, 1957–1960.
47. Abou Assi,H., El-Khoury,R., González,C. and Damha,M.J. (2017) 2′-Fluoroarabinonucleic acid modification traps G-quadruplex and i-motif structures in human telomeric DNA. *Nucleic Acids Res.*, **45**, 11535–11546.
48. Cui,Y., Kong,D., Ghimire,C., Xu,C. and Mao,H. (2016) Mutually exclusive formation of G-quadruplex and i-Motif Is a general phenomenon governed by steric hindrance in duplex DNA. *Biochemistry*, **55**, 2291–2299.
49. Michelotti,G.A., Michelotti,E.F., Pullner,A., Duncan,R.C., Eick,D. and Levens,D. (1996) Multiple single-stranded cis elements are associated with activated chromatin of the human c-myc gene in vivo. *Mol. Cell Biol.*, **16**, 2656–2669.
50. Klejevskaja,B., Pyne,A.L.B., Reynolds,M., Shivalingam,A., Thorogate,R., Hoogenboom,B.W., Ying,L. and Vilar,R. (2016) Studies of G-quadruplexes formed within self-assembled DNA mini-circles. *Chem. Commun.*, **52**, 12454–12457.
51. Annunziato,A.T. (2008) DNA packaging: nucleosomes and chromatin. *Nat. Educ.*, **1**, 26.
52. Guo,J. and Price,D.H. (2013) RNA polymerase II transcription elongation control. *Chem. Rev.*, **113**, 8583–8603.
53. Valero,J., Pal,N., Dhakal,S., Walter,N.G. and Famulok,M. (2018) A bio-hybrid DNA rotor–stator nanoengine that moves along predefined tracks. *Nat. Nanotechnol.*, **13**, 496–503.
54. Schwartz,J.J. and Quake,S.R. (2009) Single molecule measurement of the "speed limit" of DNA polymerase. *Proc. Natl. Acad. Sci. U.S.A.*, **106**, 20294–20299.
55. Jonchhe,S., Shrestha,P., Aschncio,K. and Mao,H. (2018) A new concentration jump strategy reveals the lifetime of i-Motif at physiological pH without force. *Anal. Chem.*, **90**, 3205–3210.
56. Gibbs,D., Kaur,A., Megalathan,A., Sapkota,K. and Dhakal,S. (2018) Build your own microscope: step-by-step guide for building a prism-based TIRF microscope. *Methods Protoc.*, **1**, 40.
57. Ha,T. (2001) Single-molecule fluorescence resonance energy transfer. *Methods*, **25**, 78–86.
58. Suddala,K.C., Cabello-Villegas,J., Michnicka,M., Marshall,C., Nikonowicz,E.P. and Walter,N.G. (2018) Hierarchical mechanism of amino acid sensing by the T-box riboswitch. *Nat. Commun.*,**9**, 1896.
59. Gibbs,D.R. and Dhakal,S. (2018) Single-molecule imaging reveals conformational manipulation of holliday junction DNA by the junction processing protein RuvA. *Biochemistry*, **57**, 3616–3624.
60. Lee,S., Lee,J. and Hohng,S. (2010) Single-molecule three-color FRET with both negligible spectral overlap and long observation time. *PLOS ONE*, **5**, e12270.
61. Lerner,E., Cordes,T., Ingargiola,A., Alhadid,Y., Chung,S., Michalet,X. and Weiss,S. (2018) Toward dynamic structural biology: Two decades of single-molecule Förster resonance energy transfer. *Science*, **359**, 288.
62. McKinney,S.A., Joo,C. and Ha,T. (2006) Analysis of single-molecule FRET trajectories using hidden markov modeling. *Biophys. J.*, **91**, 1941–1951.
63. Abelson,J., Blanco,M., Ditzler,M.A., Fuller,F., Aravamudhan,P., Wood,M., Villa,T., Ryan,D.E., Pleiss,J.A., Maeder,C. *et al.* (2010) Conformational dynamics of single pre-mRNA molecules during in vitro splicing. *Nat. Struct. Mol. Biol.*, **17**, 504–512.
64. Chavis,A.E., Brady,K.T., Hatmaker,G.A., Angevine,C.E., Kothalawala,N., Dass,A., Robertson,J.W.F. and Reiner,J.E. (2017) Single molecule nanopore spectrometry for peptide detection. *ACS Sensors*, **2**, 1319–1328.
65. Angevine,C.E., Seashols-Williams,S.J. and Reiner,J.E. (2016) Infrared laser heating applied to nanopore sensing for DNA duplex analysis. *Anal. Chem.*, **88**, 2645–2651.
66. Rasched,G., Ackermann,D., Schmidt Thorsten,L., Broekmann,P., Heckel,A. and Famulok,M. (2008) DNA minicircles with gaps for versatile functionalization. *Angew. Chem. Int. Ed.*, **47**, 967–970.
67. Du,Q., Vologodskaia,M., Kuhn,H., Frank-Kamenetskii,M. and Vologodskii,A. (2005) Gapped DNA and cyclization of Short DNA fragments. *Biophys. J.*, **88**, 4137–4145.
68. Phan,A.T., Guéron,M. and Leroy,J.L. (2000) The solution structure and internal motions of a fragment of the cytidine-rich strand of the human telomere, *J. Mol. Biol.*, **299**, 123–144.
69. Tsukanov,R., Tomov,T.E., Masoud,R., Drory,H., Plavner,N., Liber,M. and Nir,E. (2013) Detailed study of DNA hairpin dynamics using single-molecule fluorescence assisted by DNA origami. *J. Phys. Chem. B*, **117**, 11932–11942.
70. Sasmal,D.K., Pulido,L., Kasal,S. and Huang,J. (2016) Single-molecule fluorescence resonance energy transfer in molecular biology. *Nanoscale*, **8**, 19928–19944.
71. Majumdar,D.S., Smirnova,I., Kasho,V., Nir,E., Kong,X., Weiss,S. and Kaback,H.R. (2007) Single-molecule FRET reveals sugar-induced conformational dynamics in LacY. *Proc. Natl. Acad. Sci. U.S.A.*, **104**, 12640–12645.
72. Roy,R., Hohng,S. and Ha,T. (2008) A practical guide to single molecule FRET. *Nat. Methods*, **5**, 507–516.

73. Song,L., Hobaugh,M.R., Shustak,C., Cheley,S., Bayley,H. and Gouaux,J.E. (1996) Structure of staphylococcal α-hemolysin, a heptameric transmembrane pore. *Science*, **274**, 1859–1865.
74. Dhakal,S., Lafontaine,J.L., Yu,Z., Koirala,D. and Mao,H. (2012) Intramolecular folding in human ILPR fragment with three C-rich repeats. *PLOS ONE*, **7**, e39271.
75. Murphy,M.C., Rasnik,I., Cheng,W., Lohman,T.M. and Ha,T. (2004) Probing single-stranded DNA conformational flexibility using fluorescence spectroscopy. *Biophys. J.*, **86**, 2530–2537.
76. Xu,Y., Liu,Y. and Qian,X. (2007) Novel cyanine dyes as fluorescent pH sensors: PET, ICT mechanism or resonance effect? *J. Photochem. Photobiol. A: Chem.*, **190**, 1–8.
77. Reilly,Samantha M., Lyons,Daniel F., Wingate,Sara E., Wright,Robert T., Correia,John J., Jameson,David M. and Wadkins,Randy M. (2014) Folding and hydrodynamics of a DNA i-Motif from the c-MYC promoter determined by fluorescent cytidine analogs. *Biophys. J.*, **107**, 1703–1711.
78. Garabedian,A., Butcher,D., Lippens,J.L., Miksovska,J., Chapagain,P.P., Fabris,D., Ridgeway,M.E., Park,M.A. and Fernandez-Lima,F. (2016) Structures of the kinetically trapped i-motif DNA intermediates. *Phys. Chem. Chem. Phys.*, **18**, 26691–26702.
79. Leroy,J.L. and Esmaili,N. (2005) i-motif solution structure and dynamics of the d(AACCCC) and d(CCCCAA) tetrahymena telomeric repeats. *Nucleic Acids Res.*, **33**, 213–224.